PAPER

Solution combustion synthesis of ternary Ni/WC/C composites with efficient electrocatalytic oxygen reduction performance

Pengqi Chen, [iD] [ab] Yunxiao Tai,[a] Qingqing Fang,[a] Dang Xu,[a] Yufei Gao[a] and Jigui Cheng*[ac]

In this paper, a fast processing route involving a wet-chemical method (solution combustion synthesis, SCS) and carbonization in a CH_4 environment was demonstrated, through which nanosized Ni/WC/C powder with an average size of 80 nm was obtained. In the catalyst powder, Ni was evenly distributed and it could form NiOOH to promote catalysis, and an amorphous carbon (C) layer with a thickness of <10 nm was formed on the surface of the composite particles, improving the stability of the Ni/WC powder and promoting electron transport. Due to the characteristics of uniformity and a large specific surface area and the synergistic effect of Ni, WC, and C, this powder showed significantly improved ORR catalytic activity in alkaline solution. When the amount of Ni doping was 15 wt%, the composite powder showed the smallest particle size and the best ORR catalytic performance. Its cathode peak potential was −0.31 V and the half wave potential was −0.34 V. The number of electrons transferred in the ORR reaction was 3.6. This work provided a fast and cheap method for the preparation of multicomponent composite catalyst materials.

1. Introduction

Proton exchange membrane fuel cells (PEMFCs) are the type of fuel cell that have been developed on the largest scale at present, with the advantages of creating no environmental pollution, and having high energy conversion efficiency and high power density.[1–3] However, the cost and efficiency of the oxygen reduction reaction (ORR) at the cathode have significantly restricted the development of PEMFCs. Although Pt-based catalysts present superior ORR activity, their high price and insufficient durability under real working conditions hinder their industrialization. Non-precious metal catalysts generally present relatively stable properties in alkaline media, and many applications of non-precious metal catalysts in hydrogen evolution have been reported.[4,5] This provides the possibility for the research and development of non-precious metal catalysts for the ORR reaction, including transition-metal oxides,[6] carbides,[7] nitrides,[8] alloys,[9] *etc.* Among these materials, tungsten carbide (WC) is a kind of special catalyst, which exhibits catalytic behavior similar to that of Pt. Its large reserves and its particular insensitivity to toxic substances such

as H_2S, CO, *etc.* give it good application prospects in the field of catalysis.[10,11] Therefore, WC has attracted much attention as a catalyst and catalyst support material in recent years.

On the other hand, Fe, Co, Ni, and other transition metals, with lower prices than Pt and other precious metals, have attracted the extensive attention of researchers due to their excellent electrocatalytic activities, making it possible for non-precious-metal catalysts to replace precious-metal catalysts for large-scale commercialization.[12–14] Qian *et al.* confirmed that the use of a synthesized carbon substrate and a fine-tuned amount of a AgNi alloy could effectively prevent active nanoparticles from agglomeration and leaching during long-term use, thus allowing AgNi/NC-X to be employed as an efficient electrocatalysts for the HER.[15] Also it was reported that when Ni WC/C was used as an ORR catalyst, Ni and WC could work synergistically to form NiOOH, which had superior activity and stability during the electrooxidation of urea.[16]

In our previous study,[17] we reported the preparation of WC/C composites *via* a combustion method. A graphite carbon layer was formed on the surface of WC particles in the material, which significantly improved the ORR catalytic performance of the material in KOH solution. Moreover, there are literature studies showing that the carbon layer formed on the surface of WC not only limits the agglomeration and growth of WC, but it also improves the specific surface area of WC and makes it difficult for the internal active nanoparticles to be degraded. Carbon also has good conductivity, and it can effectively transfer electrons in reactions and contribute to catalytic

[a]School of Materials Science and Engineering, Hefei University of Technology, Hefei 230009, China. E-mail: chenpq@hfut.edu.cn

[b]National–Local Joint Engineering Research Centre of Nonferrous Metals and Processing Technology, Hefei 230009, China

[c]Research Centre for Powder Metallurgy Engineering and Technology of Anhui Province, Hefei, 230009, China. E-mail: jgcheng@hfut.edu.cn
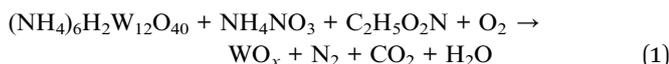
reactions.[18–21] For example, Guo *et al.* used carbon to disperse WC particles and inhibited the grain growth of WC, obtaining excellent ORR properties.[22] Ma *et al.* reported that a new type of Ni/WC@NC structure exhibited remarkable catalytic stability, which was ascribed to its high chemical stability and unique hybrid structure with hybrid nanoparticles anchored on N-doped carbon sheets.[23]

Therefore, upon summarizing the relevant literature and previous research, we assume that if a transition metal is combined with WC/C to form a ternary combination, this could present a synergistic effect that is expected to improve the catalytic activity and stability. Firstly, $NiO–WO_x$ precursor powder was prepared *via* a SCS method, and a Ni/WC/C ternary composite catalyst was formed *via in situ* carbonization under a CH_4 atmosphere. Compared with other Ni/WC preparation methods, which lead to problems such as long reaction times and uneven particle size distributions, SCS has great advantages as a liquid-phase chemical method. The reactants can be uniformly mixed at the ionic level. Therefore, the nano-composite powder is uniform. At the same time, the reaction speed is fast, and powder with a uniform pore structure and high surface activity can be prepared.[24,25] In this work, catalyst powder with excellent properties was obtained using this method. The electrocatalytic performance of the Ni/WC/C catalyst was investigated for the ORR in an alkaline medium. The chemical and physical properties of the material were investigated *via* scanning electron microscopy (SEM), X-ray diffraction (XRD), X-ray photoelectron spectroscopy (XPS), and transmission electron microscopy (TEM) studies. Cyclic voltammetry (CV) and steady-state polarization curves from the ORR were investigated using an ultra-thin catalyst layer deposited on the disk of a rotating ring-disk electrode (RRDE).

2. Experimental section

2.1 Preparation of Ni/WC/C

The reaction processes during experiments are shown as follows:

$$(NH_4)_6H_2W_{12}O_{40} + NH_4NO_3 + C_2H_5O_2N + O_2 \rightarrow \\ WO_x + N_2 + CO_2 + H_2O \quad (1)$$

$$Ni(NO_3)_2 + C_2H_5O_2N \rightarrow NiO + N_2 + CO_2 + H_2O \quad (2)$$

0.0040 mol of ammonium metatungstate (AMT) was used as the benchmark each time, and four nickel nitrate ($Ni(NO_3)_2$) samples equivalent to mass ratios of 10 wt%, 15 wt%, 20 wt%, and 25 wt% were weighed out. Other raw material weights were calculated according to the reaction equation, and they were as follows: 0.24 mol of ammonium nitrate, 0.0932 mol of glycine, and 0.0024 mol of EDTA. The weighed raw materials were added into deionized water to obtain a completely dissolved homogeneous solution system. This was put into a box furnace and heated at a constant temperature of 200 °C for two hours. The solution was concentrated, and bubbles began to form with the generation of a gel-like substance. Heating was continued, and the gelatinous substance reacted violently with the release of

a large amount of gas. Then the experimental raw materials were burned. It took only a few seconds to complete the entire combustion reaction. When the reaction was over, the mixture was cooled down to obtain loose bulk products, which corresponded to the four types of nano-oxide precursor powder.

The prepared precursor powder was placed in an alumina porcelain boat and placed in a sintering furnace with a mixed gas atmosphere of 20% CH_4 and 80% H_2, and the precursor was reduced and carbonized. It was heated up to 850 °C, held for 6 h, and cooled down to room temperature; in this way, Ni/WC/C composite powder could be obtained.

2.2 Characterization

In this study, X-ray diffraction analysis of the powder samples was carried out using a D/max-γB instrument produced by Japan Rigaku. The test conditions used Cu Kα radiation ($\lambda = 1.5406$ Å) and a scan rate of $10°$ min^{-1}. The instruments used to analyze the morphology of Ni/WC/C powder were an SU8020 field emission scanning electron microscope (FESEM) and a Tecnai G^2 F20 transmission electron microscope (TEM). The pore structure and pore volume of Ni/WC/C powder were tested *via* the BET method using an ASAP2020 physical adsorption and desorption instrument. X-ray photoelectron spectroscopy (XPS) studies were performed with a Thermo ESCALAB250Xi spectrometer.

2.3 Electrochemical performance testing

A solution was prepared *via* mixing 10 mg of catalyst with 350 μL of deionized water, 600 μL of isopropyl alcohol, and 50 μL of Nafion (5 wt%), and this mixture was treated with ultrasound for 0.5 h. 15 μL of catalyst solution was added to the glassy carbon substrate of the working electrode in three drops with catalyst loading of 25.48 μg cm^{-2}. The working electrode was obtained after drying. The electrochemical properties of the samples were measured using a three-electrode set-up. 0.1 mol L^{-1} KOH solution at room temperature was used as electrolyte solution. N_2 and O_2 were introduced for 40 min before testing to ensure that testing was performed under conditions of N_2 saturation and O_2 saturation, respectively. Cyclic voltammetry (CV) analysis in this study was carried out in the range from 0.1 to -0.8 V (*vs.* Ag/AgCl), and the scan rate was 50 mV s^{-1}. Linear sweep voltammetry (LSV) analysis in this study was carried out in the range from 0.1 to -0.6 V (*vs.* Ag/AgCl), and the scan rate was 10 mV s^{-1}.

3. Results and discussion

3.1 Characterization of the synthesized powder

Fig. 1 shows the XRD patterns of precursors synthesized with different Ni ratios. Upon analyzing the XRD patterns of the four precursor powder samples, it could be seen that the main components of the precursor powder samples were $W_{18}O_{49}$ and a small amount of Ni. The results showed that three strong peaks in the four precursor patterns were located at 2θ values of $23.47°$, $23.77°$, and $24.39°$, which were the typical characteristic peaks of $W_{18}O_{49}$, corresponding to the (010), (103), and (−502)
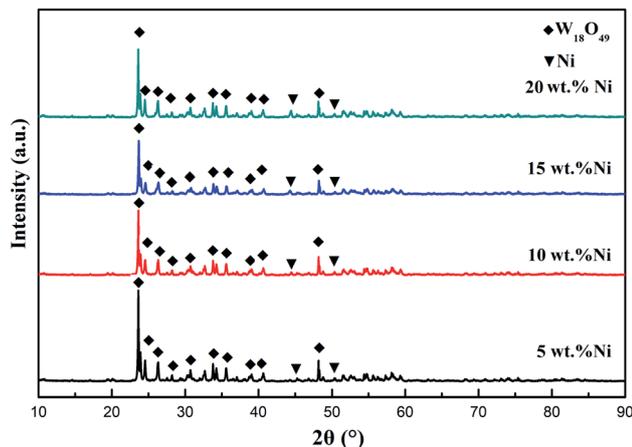
Fig. 1 XRD patterns of precursors with different amounts of Ni doping (5 wt%, 10 wt%, 15 wt%, and 20 wt%).

crystal faces of violet tungsten (JCPDS no. 71-2450). At the same time, two diffraction peaks appeared at 2θ values of $44.31°$ and $51.4°$, respectively. With an increase in the Ni content, these diffraction peaks gradually became more obvious. Upon comparison with the standard PDF card, the two diffraction peaks were seen to be consistent with the (111) and (200) crystal faces of Ni (fcc structure, JCPDS no. 04-0850). It was shown that the phase composition was Ni, and no NiO or NiO_2 was found in the XRD patterns. This may result from the fact that the solution combustion reaction is essentially a redox reaction between nitrate and the fuel. Glycine was a reducing agent in the combustion system. When the amount of glycine was high, a large amount of reducing gas was produced, due to the

reducibility of fuel, making the furnace an oxygen-poor environment and preventing the reactant from contacting with oxygen directly. Finally, $W_{18}O_{49}$ was generated with a large number of defects and Ni oxides were reduced due to the strong electronegativity of Ni. Kumar $et\ al.$ also found in an earlier study that when enough glycine was added, NiO was completely reduced to produce Ni.[26]

The morphologies of precursors prepared using different amounts of Ni doping are shown in Fig. 2. The results showed that the four powder samples were porous because a large amount of gas was released during precursor preparation, and this increased the specific surface area of the precursor. When the Ni content was 10 wt%, the powder was mainly rod-shaped. In addition, there was a small amount of needle-like powder, whose length was about 2–3 μm with a diameter of about 100 nm. With an increase in the amount of Ni doping, the powder gradually adopted the shape of short rods, and the length became about 1 μm with a diameter of 200 nm (15 wt% Ni).

Ni/WC samples were prepared via a temperature-programmed method, and the XRD patterns of the samples are shown in Fig. 3. It can be seen from Fig. 3 that the sample was mainly composed of a WC phase, with small amounts of Ni and C phases. When the content of Ni was 5 wt%, the Ni peaks were not obvious, which might result from the fact that the added amount of Ni was too small to be detected. The WC phase was dominant, and the peak shapes were sharp, indicating that WC powder with good crystallinity was formed. Previous literature reports showed that the addition of Ni can contribute to the carbonization of oxides.[27] Therefore, the addition of a small amount of Ni helped $W_{18}O_{49}$ to form WC powder with high
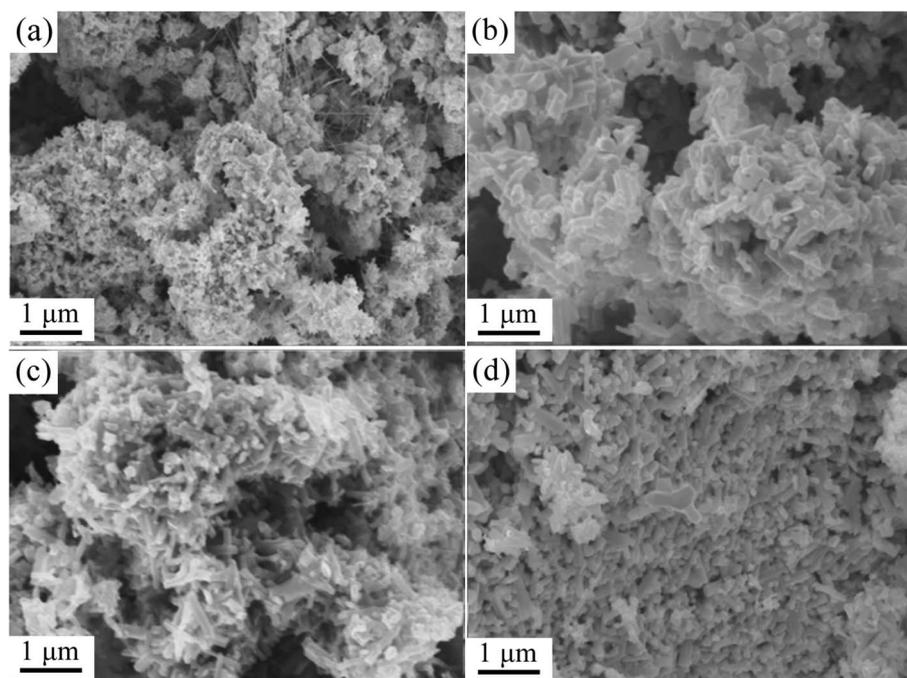

Fig. 2 SEM images of precursors prepared with different amounts of Ni: (a) 5 wt%, (b) 10 wt%, (c) 15 wt%, and (d) 20 wt%.
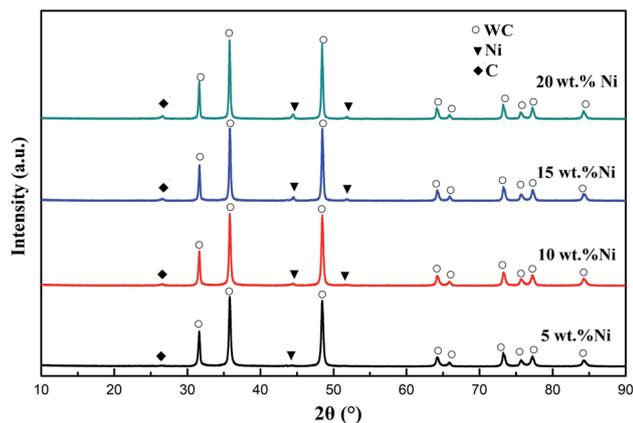
Fig. 3 XRD patterns of Ni/WC composite powder samples with different amounts of Ni: 5 wt%, 10 wt%, 15 wt%, and 20 wt%.

crystallinity at a lower temperature. The diffraction peaks at 2θ values of $44.42°$ and $51.78°$ indicated the existence of a metallic Ni phase. The peaks at 2θ values of $31.60°$, $35.72°$, $48.26°$, and $73.38°$ were consistent with the (001), (100), (101), and (111) crystal planes of WC with a close-packed hexagonal structure (JCPDS no. 73-0471). A diffraction peak from C ($2\theta = 26.6°$) was also observed in Ni/WC samples. This was because the presence of a transition metal such as Ni was helpful for the decomposition of methane and the conversion of amorphous carbon into graphitic carbon.[28,29]

Corresponding to the phase change, the morphologies of the catalyst particles also changed with an increase in the Ni content (Fig. 4). When the added amount of Ni was 5 wt%, the morphology of the particles was regular with good crystallinity and a uniform particle size. The size of a single particle was

about 300 nm. This might be because Ni could promote the decomposition of methane,[30] increasing the carbon concentration in the tubular furnace, and promoting the carbonization reaction. At a relatively low reaction temperature, WC powder with uniform size could be obtained. When the content of Ni was 10 wt%, there were obvious small particles alongside the large particles. The size of the large particles was about 300 nm, and that of the small particles was about 100 nm. With an increase in the Ni content, the particles gradually became fine and uniform. When the content of Ni was 15–20 wt%, the particle size was less than 200 nm. It was found that the addition of Ni could refine the WC grains and improve the catalytic activity during the ORR.

Fig. 5 shows the nitrogen adsorption–desorption curves of WC powder samples with different amounts of Ni. It can be seen from the plots that the adsorption and desorption curves of the four samples showed H4-type hysteresis loops and type-IV isotherms. This indicated that the four samples had obvious mesoporous structures. When the amount of Ni added was 20 wt%, adsorption was not obvious at low relative pressure values ($P/P_0 < 0.2$), which suggested that there were micropores in the sample. When the relative pressure was 0.45–0.95, an obvious hysteresis loop appeared, indicating that the sample was a typical mesoporous structure with a pore size of 4.57 nm. Also, at high relative pressures ($P/P_0 > 0.95$), the curve showed an upward trend, which suggested the existence of large pores. Based on the BET model, the total pore volumes and specific surface areas of the four samples were calculated, and the results are shown in Table 1. The pore size, pore volume, and specific surface area of the catalyst increased significantly when the amount of Ni was increased from 5 wt% to 15 wt%, which was consistent with the SEM results. Continuing to increase the Ni content further, the pore size decreased slightly. This might
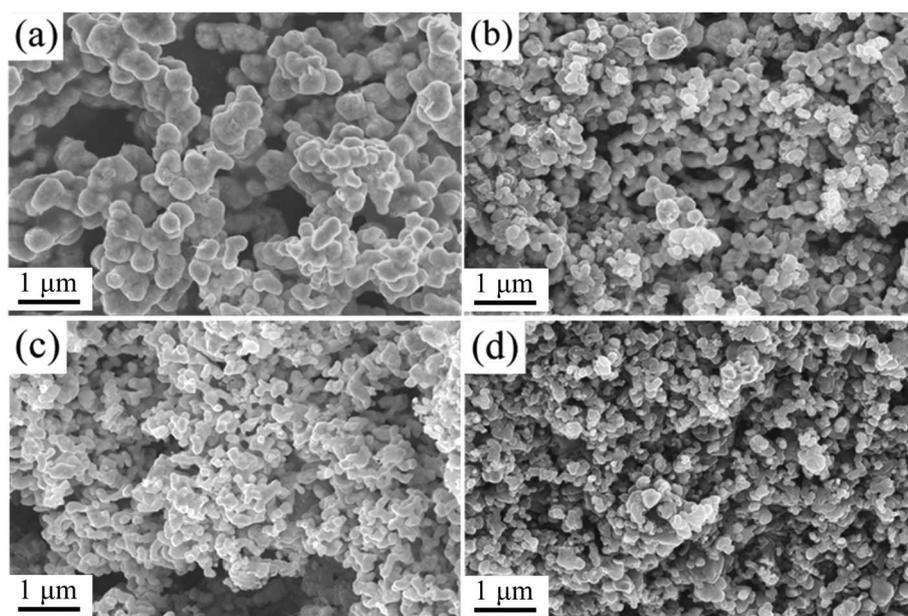

Fig. 4 SEM images of Ni/WC composite powder with different amounts of Ni: (a) 5 wt%, (b) 10 wt%, (c) 15 wt%, and (d) 20 wt%.
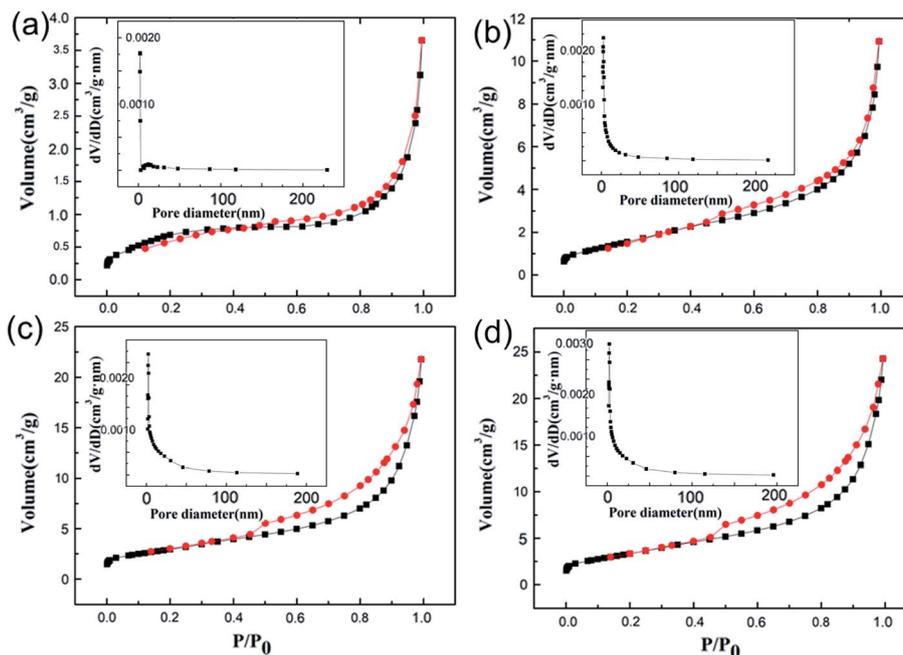
Fig. 5 N_2 adsorption−desorption curves of WC powder samples with different amounts of Ni: (a) 5 wt%, (b) 10 wt%, (c) 15 wt%, and (d) 20 wt%. The insets show the pore size distributions.

Table 1 Pore diameter, pore volume, and specific surface area data from Ni/WC composite powder samples with different amounts of Ni

Ni content (wt%)	Pore diameter (nm)	Volume ($\times 10^{-3}$ cm^3 g^{-1})	Specific surface area (m^2 g^{-1})
5	4.36	5.82	2.66
10	6.67	10.07	6.04
15	7.76	35.13	12.49
20	7.58	39.62	10.77

result from an increase in Ni, which caused the carbonization reaction to be more violent with an even higher degree of carbonization. Therefore, the skeleton of the material shrank dramatically and the pore size decreased.

The addition of Ni further refined the crystal grains of the catalyst, increased the specific surface area and the number of surface atoms, and resulted in the formation of a large number of unsaturated bonds; this was conducive to the adsorption and reaction of oxygen molecules on the catalyst surface. At the same time, the porous structure is beneficial for the rapid passage of various ions in the ORR catalytic process, which should improve the catalytic efficiency.[31]

The morphologies and structures of the prepared Ni/WC/C powder samples were observed *via* transmission electron microscopy (TEM). The results for the sample with 10 wt% Ni are shown in Fig. 6. It can be seen from Fig. 6(a) that the size of the Ni/WC nanoparticles was about 80 nm, and the outer layer was tightly wrapped with a <10 nm-thick carbon layer. This was due to the fact that Ni and W could catalyze the graphitization reaction of amorphous carbon[29,32] to form a surface carbon

layer, which significantly improved the stability of the Ni/WC nanoparticles. From element mapping, the mixed distribution of Ni and WC in the powder further proved that multiple Ni/WC interfaces existed in the powder, which could promote material transfer between Ni and WC, thus being conducive to catalytic reactions.[33]

In order to further characterize the elemental composition of Ni/WC/C powder, XPS analysis was carried out. The W, Ni, and C XPS spectra from the sample with 10 wt% Ni are shown in Fig. 7(a)–(c), respectively. The high-resolution Ni 2p XPS spectrum showed two distinct peaks at 852 eV and 872 eV, corresponding to Ni 2p$_{3/2}$ and Ni 2p$_{1/2}$, respectively. The peaks at 857.4 eV and 876.2 eV indicated partial oxidation on the Ni surface.[34] It could be seen from Fig. 7(a) that there was a doublet of strong signals at 34.3 eV and 31.6 eV (W^{2+}), indicating the existence of WC, while the peaks at 37.5 eV and 35.2 eV corresponded to W^{6+} (WO$_x$), indicating that WC also showed signs of oxidation.[35] The oxidation of Ni and WC might result from the fact that the existence of Ni reduced the particle size of the product powder, increasing the surface activity and making it easier to react with oxygen. This was consistent with results reported in the earlier literature showing that as MoC$_x$ and WC$_x$ particles became larger, the oxidation resistance was enhanced, and WC was partially oxidized to form a passivation layer, which improved the acid and alkali resistance.[36] The C 1s XPS spectrum showed two peaks at 284.7 eV and 286.3 eV, corresponding to C=C and C=O, respectively. The existence of C=C further indicated the existence of a carbon layer on the sample surface, which was consistent with the previous conclusions.
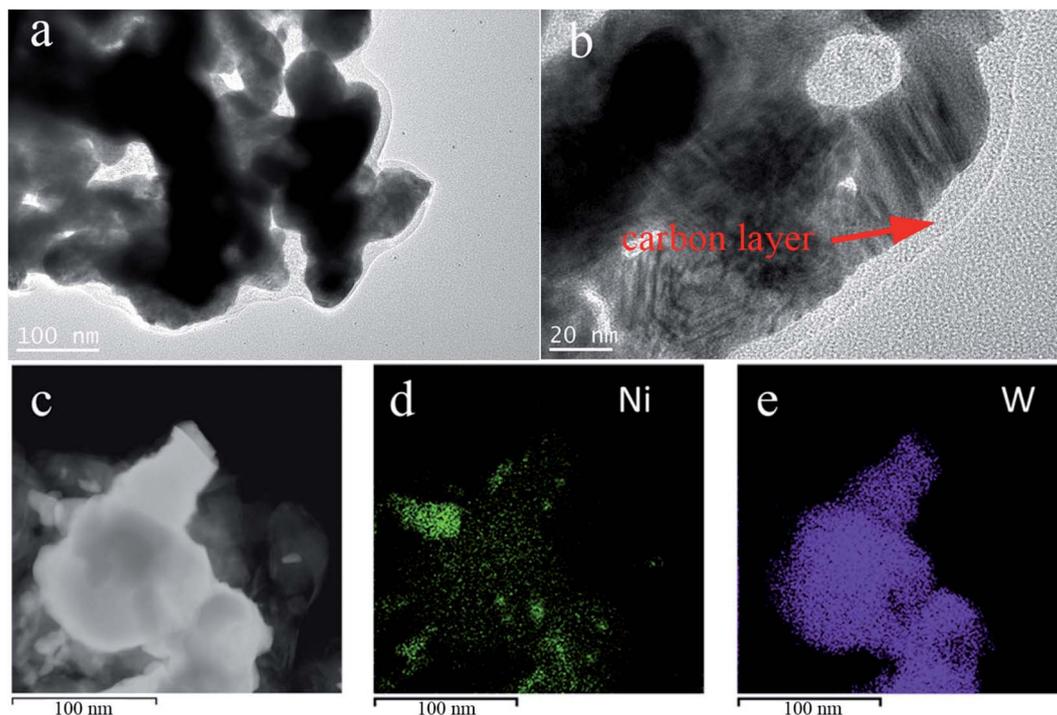
Fig. 6 (a, b) TEM images of Ni/WC powder and (c, d, and e) element mapping of the Ni/WC/C composite powders (10 wt% Ni/WC).

3.2 Performance of Ni/WC/C powder

3.2.1 Cyclic voltammetry analysis. The electrolyte solution used in experiments was 0.1 mol L^{-1} KOH solution, and experiments were carried out under the condition of oxygen saturation, using a traditional three-electrode system. The CV curves based on the experimental data are shown in Fig. 8. From the curves, obvious oxygen reduction peaks could be observed under O_2-saturation conditions, indicating that the samples presented oxygen reduction activity. Compared with the potentials of the reduction peaks of the samples, it could be found that when the added amounts of Ni were 5, 10, 15, and 20 wt%, the reduction peak potentials were −0.39, −0.34, −0.27, and −0.35 V, respectively. The corresponding current densities were 0.4, 0.5, 0.42, and 0.6 mA cm^{-2}, respectively.
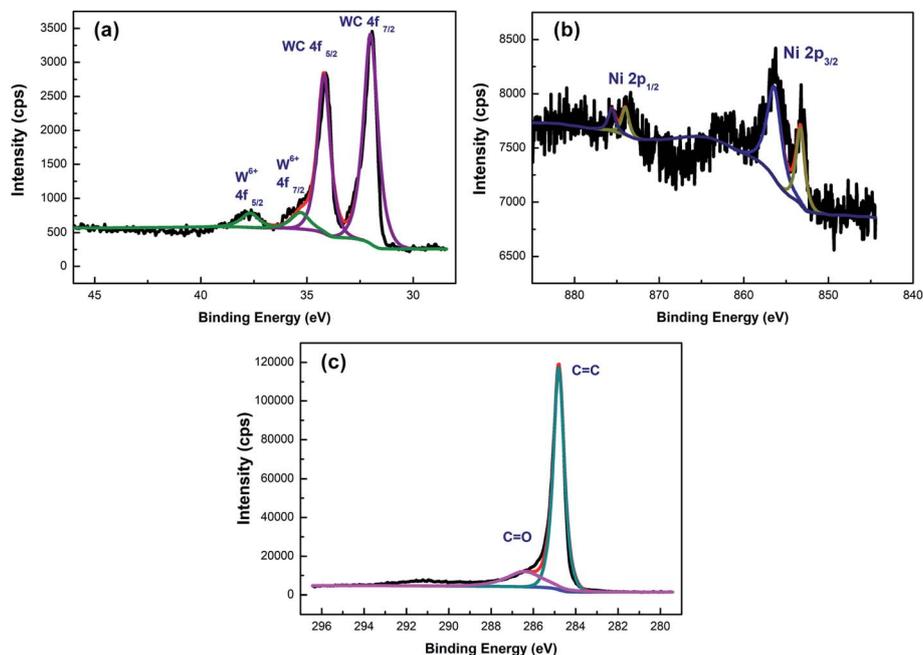

Fig. 7 High-resolution XPS spectra of Ni/WC powder (10 wt% Ni/WC): (a) W, (b) Ni, and (c) C.
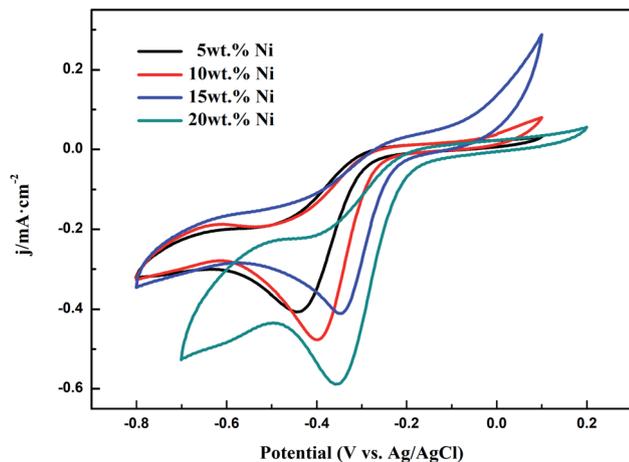
Fig. 8 CV curves from Ni/WC/C powder samples with Ni different content levels: 5 wt%, 10 wt%, 15 wt%, and 20 wt%.

Obviously, when the amount of added Ni was 15 wt%, the oxygen reduction peak potential was the most positive, indicating that the oxygen reduction reaction could take place at a lower potential. This sample had the smallest overpotential and the best catalytic activity for oxygen reduction.

3.2.2 Linear sweep curve analysis. The catalytic activities of the samples were characterized using a rotating disk electrode (RDE). The test was carried out in 0.1 M KOH electrolyte solution saturated with O_2. The obtained LSV curves are shown in Fig. 9. The half-wave potentials of the Ni/WC composite powder samples were −0.33, −0.31, −0.29, and −0.30 V when the Ni content was 5, 10, 15, and 20 wt%, respectively. This result is consistent with the CV test results. The limiting diffusion current densities of the samples were 0.9, 1.3, 1.35, and 1.1 mA cm^{-2}, respectively. The data above showed that the prepared catalyst had the maximum half-wave potential and maximum diffusion current density when the added amount of Ni was 15 wt%. Combined with the performance results from blank pure WC experimental reported previously,[17] we can conclude
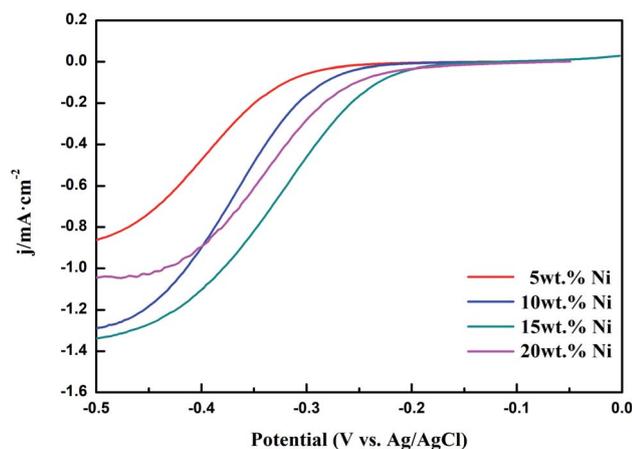
that Ni doping can effectively improve the ORR performance of WC, and the performance shows a trend of first increasing and then decreasing as the added amount is increased.

In addition, polarization curves of the 15 wt% Ni/WC/C catalyst at different speeds (400 rpm, 900 rpm, 1600 rpm, and 2500 rpm) were measured, as shown in Fig. 10. The right panel shows the K–L plot based on the polarization curves, which was used to characterize the number of electrons transferred to O_2 molecules in the reaction. The calculation formulas[17] are as follows:

$$\frac{1}{J} = \frac{1}{J_k} + \frac{1}{J_L} = \frac{1}{J_k} + \frac{1}{B\omega^{1/2}} \tag{3}$$

$$B = 0.2nFC_0(D_0)^{2/3}\nu^{-1/6} \tag{4}$$

$$J_k = nFkC_0 \tag{5}$$

In these equations, J represents the measured current density; J_k refers to the kinetic current density; B is the slope of the K–L plot; ω refers to the rotation speed (rpm); and F is the Faraday constant. In our system (0.1 mol L^{-1} KOH solution), C_0 is the concentration of O_2, with a value of 1.2×10^{-3} mol cm^{-3}; D_0 is the dispersion coefficient of O_2, which is 1.0×10^{-5} cm s^{-1}; and ν is the kinetic viscosity of the electrolyte (0.01 cm^2 s^{-1}). Based on our calculations, the number of electrons transferred in the ORR reaction is 3.6, which indicates that a two-electron transfer process and a four-electron transfer process occur simultaneously in the ORR, and the four-electron transfer is the main reaction process. This is similar to some existing research. For example, Xu *et al.* developed a multifunctional carbon-encapsulated Ni@NiO nanocomposite (Ni@NiO@C) which was stable and could be used in methanol and alkaline fuel cells. Its ORR followed a quasi-four-electron pathway, similar to that of Pt/C.[19] All of the above test results prove that the 15 wt% Ni/WC catalyst prepared *via* this method has excellent catalytic activity for oxygen reduction.

3.3 Mechanism discussion

We think that the above performance is mainly due to two reasons, as follows.

(1) The excellent physical properties of the powder. A solution combustion synthesis method was used in this study. All raw materials were soluble in water and could achieve ion-level mixing. Ni and WC in the obtained powder could be mixed very uniformly without obvious agglomeration. Meanwhile, this method generated a large amount of gas during the reaction, which was quickly released in a short time to form powder with a suitable pore structure. Therefore, these powder samples had large specific surface areas and could present good performance. Similar results have been reported previously. Song *et al.* used g-C$_3$N$_4$-restricted particle growth to obtain a Ni–WC catalyst with a high BET surface area *via* heat treatment, which also led to remarkable material performance.[37]

(2) The synergistic effects of Ni, WC and C. The presence of elemental Ni promoted the decomposition of methane, so that WC powder could be formed quickly at a lower temperature,
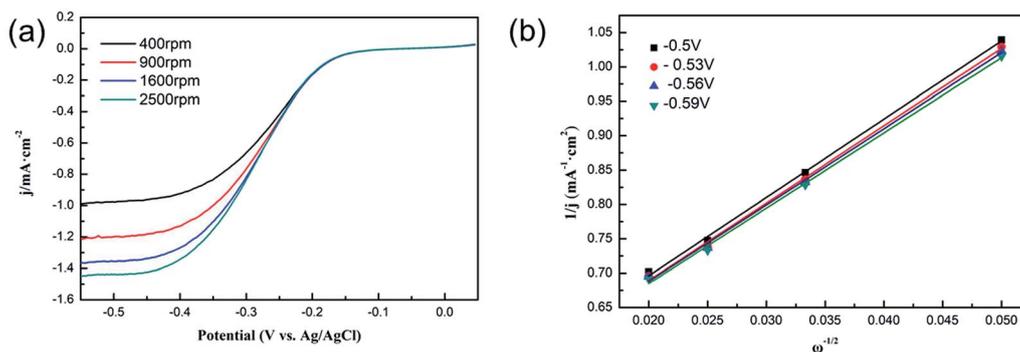

Fig. 9 LSV curves from Ni/WC/C powder samples with different amounts of Ni: 5 wt%, 10 wt%, 15 wt%, and 20 wt% (rotation speed: 1600 rpm).

Fig. 10 Polarization curves of 15wt% Ni/WC catalyst at different speeds (400 rpm, 900 rpm, 1600 rpm, 2500 rpm).

and the prepared WC powder had fine particles and a uniform element distribution. The fine particles increased the number of surface atoms, and a large number of the surface atoms were in an unsaturated chemical valence state, forming many dangling bonds; this improved the surface activity of the catalyst, enhanced the adsorption capacity of oxygen on the surface, and made the oxygen reduction reaction more efficient. In addition, WC had a broader unoccupied d band (or, more likely, a hybrid tungsten 5d and carbon 2p band) than tungsten. This property enabled tungsten carbide to attract the outer electrons of nickel atoms, which caused nickel to lose electrons and reach its active oxide state (NiOOH).[18] Therefore, tungsten carbide could be used together with nickel as a cocatalyst to improve activity during the oxidation process.

In addition, a carbon layer several nanometers thick was formed upon carbonization under a CH_4 atmosphere under Ni catalysis. The existence of a graphite layer on the surface prevented the growth of Ni/WC grains, improved the stability of Ni/WC powder, and promoted electron transport. In a word, the presence of Ni, WC, and C led to a synergistic effect.

4. Conclusions

In summary, a nanosized Ni/WC/C composite catalyst material was successfully prepared *via* a solution combustion *in situ* carbonization method. As was evidenced, with an increase in the Ni content, the particles of WC gradually became finer, and the size distribution was more uniform. The Ni/WC/C composite prepared upon doping with 15 wt% Ni showed a typical mesoporous structure with a pore diameter of approximately <10 nm, which was conducive to the rapid movement of ions in the oxygen reduction reaction. It had the most positive reduction peak potential of −0.31 V and the most positive half-wave potential of −0.34 V, leading to the least hindrance in terms of electron transfer and the best catalytic activity for oxygen reduction. This excellent performance is attributed to the unique physical properties of the powder and the synergistic effect of Ni, WC, and C. We hope that our work will help to open up new strategies for the design of efficient noble-metal-free electrocatalysts, especially composite examples.

Conflicts of interest

No conflict of interest exists in the submission of this manuscript, and the manuscript is approved by all authors for publication. I would like to declare on behalf of my co-authors that the work described is not under review at any other publication. We confirm that all authors have checked the manuscript and have agreed to the submission.

Acknowledgements

References

1 M. P. Browne, Z. Sofer and M. Pumera, *Energy Environ. Sci.*, 2019, **12**, 41–58.
2 R. Sirirak, B. Jarulertwathana, V. Laokawee, W. Susingrat and T. Sarakonsri, *Res. Chem. Intermed.*, 2016, **43**, 2905–2919.
3 M. Liu, Z. Zhao, X. Duan and Y. Huang, *Adv. Mater.*, 2019, **31**, e1802234.
4 D. M. Morales, M. A. Kazakova, S. Dieckhöfer, A. G. Selyutin, G. V. Golubtsov, W. Schuhmann and J. Masa, *Adv. Funct. Mater.*, 2019, **30**, 1905992.
5 K. Jayasayee, J. A. R. V. Veen, T. G. Manivasagam, S. Celebi, E. J. M. Hensen and F. A. de Bruijn, *Appl. Catal., B*, 2012, **111–112**, 515–526.
6 A. I. Large, S. Wahl, S. Abate, I. da Silva, J. J. Delgado Jaen, N. Pinna, G. Held and R. Arrigo, *Catalysts*, 2020, **10**, 1289.
7 X. H. Yan, P. Prabhu, H. Xu, Z. Meng, T. Xue and J. M. Lee, *Small Methods*, 2019, **4**, 1900575.
8 Y. Dong, Y. Deng, J. Zeng, H. Song and S. Liao, *J. Mater. Chem., A*, 2017, **5**, 5829–5837.
9 C. Kim, F. Dionigi, V. Beermann, X. Wang, T. Moller and P. Strasser, *Adv. Mater.*, 2019, **31**, e1805617.
10 Y. T. Xu, X. Xiao, Z. M. Ye, S. Zhao, R. Shen, C. T. He, J. P. Zhang, Y. Li and X. M. Chen, *J. Am. Chem. Soc.*, 2017, **139**, 5285–5288.

11 P. Xiao, X. Ge, H. Wang, Z. Liu, A. Fisher and X. Wang, *Adv. Funct. Mater.*, 2015, **25**, 1520–1526.

12 P. Xu, W. Chen, Q. Wang, T. Zhu, M. Wu, J. Qiao, Z. Chen and J. Zhang, *RSC Adv.*, 2015, **5**, 6195–6206.

13 S. Bukola, B. Merzougui, A. Akinpelu and M. Zeama, *Electrochim. Acta*, 2016, **190**, 1113–1123.

14 Y. Liu, H. Jiang, Y. Zhu, X. Yang and C. Li, *J. Mater. Chem., A*, 2016, **4**, 1694–1701.

15 D. Chen, C. Han, Q. Sun, J. Ding, Q. Huang, T.-T. Li, Y. Hu, J. Qian and S. Huang, *Green Energy Environ.*, 2021, DOI: 10.1016/j.gee.2021.04.003.

16 L. Wang, S. Zhu, N. Marinkovic, S. Kattel, M. Shao, B. Yang and J. G. Chen, *Appl. Catal., B*, 2018, **232**, 365–370.

17 Y. Gao, J. Cheng, P. Chen, B. Wei, D. Gao and D. Xu, *New J. Chem.*, 2020, **44**, 4004–4010.

18 L. Wang, M. Li, Z. Huang, Y. Li, S. Qi, C. Yi and B. Yang, *J. Power Sources*, 2014, **264**, 282–289.

19 D. Xu, C. Mu, B. Wang, J. Xiang, W. Ruan, F. Wen, X. Du, Z. Liu and Y. Tian, *Sci. China Mater.*, 2017, **60**, 947–954.

20 M. Nunes, D. M. Fernandes, M. V. Morales, I. Rodríguez-Ramos, A. Guerrero-Ruiz and C. Freire, *Catal. Today*, 2020, **357**, 279–290.

21 Y. Mei, T. T. Li, J. Qian, H. Li, M. Wu and Y. Q. Zheng, *Chem. Commun.*, 2020, **56**, 13393–13396.

22 J. Guo, Z. Mao, X. Yan, R. Su, P. Guan, B. Xu, X. Zhang, G. Qin and S. J. Pennycook, *Nano Energy*, 2016, **28**, 261–268.

23 Y.-Y. Ma, Z.-L. Lang, L.-K. Yan, Y.-H. Wang, H.-Q. Tan, K. Feng, Y.-J. Xia, J. Zhong, Y. Liu, Z.-H. Kang and Y.-G. Li, *Energy Environ. Sci.*, 2018, **11**, 2114–2123.

24 A. Varma, A. S. Mukasyan, A. S. Rogachev and K. V. Manukyan, *Chem. Rev.*, 2016, **116**, 14493–14586.

25 P. Chen, M. Qin, Z. Chen, B. Jia and X. Qu, *RSC Adv.*, 2016, **6**, 83101–83109.

26 A. Kumar, E. E. Wolf and A. S. Mukasyan, *AIChE J.*, 2011, **57**, 3473–3479.

27 N. Ji, T. Zhang, M. Zheng, A. Wang, H. Wang, X. Wang and J. G. Chen, *Angew. Chem., Int. Ed.*, 2008, **47**, 8510–8513.

28 L. Song, T. Wang, Y. Wang, H. Xue, X. Fan, H. Guo, W. Xia, H. Gong and J. He, *ACS Appl. Mater. Interfaces*, 2017, **9**, 3713–3722.

29 J. Tang, R. R. Salunkhe, J. Liu, N. L. Torad, M. Imura, S. Furukawa and Y. Yamauchi, *J. Am. Chem. Soc.*, 2015, **137**, 1572–1580.

30 A.-S. Al-Fatesh, S. Barama, A.-A. Ibrahim, A. Barama, W.-U. Khan and A. Fakeeha, *Chem. Eng. Commun.*, 2017, **204**, 739–749.

31 J.-X. Feng, J.-Q. Wu, Y.-X. Tong and G.-R. Li, *J. Am. Chem. Soc.*, 2018, **140**, 610–617.

32 T. Wang, J. Tang, X. Fan, J. Zhou, H. Xue, H. Guo and J. He, *Nanoscale*, 2014, **6**, 5359–5371.

33 B. Wu and N. Zheng, *Nano Today*, 2013, **8**, 168–197.

34 L. Ji, C. Lv, Z. Chen, Z. Huang and C. Zhang, *Adv. Mater.*, 2018, **30**, 1705653.

35 H. Yan, Y. Xie, Y. Jiao, A. Wu, C. Tian, X. Zhang, L. Wang and H. Fu, *Adv. Mater.*, 2018, **30**, 1704156.

36 D. R. Stellwagen and J. H. Bitter, *Green Chem.*, 2015, **17**, 582–593.

37 D. Song, J. Shin, Y. Lee, Y. Kwon, J. Lim, E.-J. Kim, S. Oh, M. Kim and E. Cho, *ACS Appl. Energy Mater.*, 2019, **2**, 3452–3460.